JOURNAL OF SPACECRAFT AND ROCKETS
Vol. 45, No. 2, March–April 2008

Numerical Aerodynamic Investigations on Missile Yawing Control Using Nose-Mounted Flow Effectors

S. Chen*
National Research Council Canada, Ottawa, Ontario K1A 0R6, Canada
D. Corriveau†
Defence Research and Development Canada—Valcartier, Quebec, Quebec G3J 1X5, Canada
and
S. McIlwain*
National Research Council Canada, Ottawa, Ontario K1A 0R6, Canada

DOI: 10.2514/1.32549

Computational studies were performed for supersonic flow at a Mach number $M = 1.5$ past a generic slender body equipped with miniature flow effectors on its nose cone. Various flow-effector configurations were studied and compared with wind-tunnel data. The numerical results predicted the details of how the vortex systems were changed by the presence of the flow effectors, thereby affecting the side force magnitude. In general, the computationally determined force coefficients were in reasonable agreement with the experimental data. Both the numerical and wind-tunnel results showed that the peak side forces occurred at an angle of attack of approximately 17 deg, and the maximum side force occurred when the flow effector was situated in a forward position and on the side of the body at an angular position located 45 deg from the top of the missile. The numerical studies also showed that the side forces induced by the flow effectors could be as high as 25% of the normal forces on average. This supports the idea of using small devices on the nose of slender bodies to control the side forces.

Nomenclature

C_A	=	axial force coefficient
C_{MY}	=	lateral (or side) moment coefficient
C_N	=	normal force coefficient
C_P	=	pressure coefficient
C_Y	=	lateral (or side) force coefficient
D	=	diameter of the missile base, m
H	=	height of the flow effector, m
M_∞	=	freestream Mach number
P_∞	=	freestream pressure, Pa
R_e	=	Reynolds number
r	=	radius of the missile surface curvature, m
T_∞	=	freestream temperature, K
t	=	thickness of the flow effector, m
u_τ	=	friction velocity, m/s
X_{cp}	=	pressure center in the axial direction referenced to the base of the missile body, C_{MY}/C_N
x_n	=	axial location starting from the tip of the missile nose, m
w	=	width of the flow effector, m
y^+	=	dimensionless normal distance of the first grid point from the wall, $u_\tau y/\nu$
ν	=	kinematic molecular viscosity, m^2/s
ϕ	=	azimuthal angle of the flow effector with respect to the missile body, deg

I. Introduction

THERE is a great interest in reducing the weight and volume of the missiles to enhance their performance. One approach that could lead to significant reductions in weight and volume is the use of miniature flow effectors (FEs) as an alternative to traditional missile control surfaces. The idea is to place the miniature flow effectors on the nose surface of the missiles to perturb the flow and thus amplify or create asymmetries in the flow with the objective of generating aerodynamic forces.

Asymmetrical vortex shedding from a slender body, such as a missile, at high angles of attack causes significant induced yawing moments due to the pressure differentials across the body. Many researchers have concluded that this problem is caused by microasymmetries on the surface of the nose cone, such as small dents, cracks in the paint, and other microscopic imperfections near the tip of the nose cone [1,2]. The extent and magnitude of such flow asymmetries are subject to parameters such as the bluntness of the forebody, Reynolds number, roll angle, and angle of attack. One goal of flow control research on missiles has been to eliminate or reduce the asymmetrical separation of the flow off the nose cone. However, asymmetrical flows could also be used to provide active missile control. Smart structures could be embedded in the body of flight vehicles to manipulate the boundary layer and vortices and to provide the required control flexibility.

The concept of using miniature FEs to improve the efficiency of flow control has been investigated for the last decade. In recent years, miniature FE devices for missiles have been studied extensively at the experimental level [1,2]. Patel et al. [1] successfully stabilized a tangent ogive projectile model at high angles of attack. They used colocated sensors and an actuator that controlled the asymmetrical vortex formation with deployable flow control devices at subsonic conditions. Garon et al. [3] used free-flight experimental technology to investigate the effect of microelectromechanical systems (MEMS)-type protuberances at Mach numbers ranging from 0.8 to 2.3. The test data showed an increase in drag due to the protuberances in the supersonic regime, but there were no noticeable effects on the normal force or pitching moment; in the subsonic regime, there was little change in the drag, but a noticeable change in the normal force and pitching moment. However, these free-flight tests did not study the effect of side forces induced by the MEMS-type devices, and numerical studies were very sparse in this area.

For moderate-to-high angles of attack, slender bodies impart nonsymmetric vortices in the regions close to the forebody of the missiles. Appropriately designed miniature flow control devices located strategically close to the nose may exploit these asymmetric

Received 1 June 2007; revision received 29 August 2007; accepted for publication 4 October 2007.

*Research Officer, Institute for Aerospace Research, 1200 Montreal Road.
†Defence Scientist, 2459 Boulevard Pie-XI Nord.

vortices. The ability of these passive devices to project lateral control is determined by their locations with respect to the nose and by their sizes. Based on these ideas, Defence Research and Development Canada—Valcartier (DRDC Valcartier) and the Institute for Aerospace Research (IAR) at the National Research Council Canada (NRC) initiated a multidisciplinary project to study the issues surrounding supersonic missile flight control using miniaturized control actuation systems.

This paper will present and discuss the computational fluid dynamics (CFD) flow-effector calculations that were performed using the numerical code SPARC. The computations were performed for a generic slender-body configuration supporting a number of rectangular-key-shaped flow effectors at different locations. The parametric study involved different numbers and sizes of such devices at a variety of locations to correspond with the wind-tunnel experiments against which the computational data were compared. The objective of the study is to determine for which flow-effector configurations significant side force can be generated at moderate angles of attack at supersonic freestream conditions.

II. Problem Definition

The baseline geometry was a slender body with a three-caliber round-nosed cone followed by a 10-caliber cylindrical afterbody (Fig. 1) The FEs were situated at a distance of $x_n/D = 0.844$ (front row) or $x_n/D = 1.268$ (back row) from the nose tip to the front of the FE, where the reference length D was the diameter of the cylindrical body. Each FE was a rectangular key with blunt edges. The FEs extended from the body to a height of $H/D = 0.033$ and had a width of $w/D = 0.089$ and a thickness of $t/D = 0.026$.

The present study focused on four FE configurations. Figure 2 describes their locations with respect to the studied geometry, where ϕ denotes their azimuthal angles as measured clockwise from the z axis when viewed from the front of the missile. For each of the single-FE and triple-FE configurations, there were two FE positions: one with $\phi = 135$ deg and the other with $\phi = 90$ deg. For the triple-FE configuration, the azimuthal angle was measured relative to the position of the center FE, and the other two were spaced 30 deg on either side of the central FE. For convenience, the boxed notations for these four FE configurations shown in the figure will be used frequently in the rest of this paper. The only rear-row configuration studied numerically consisted of a single-FE configuration with $\phi = 135$ deg. The freestream flow conditions were Mach number $M_\infty = 1.5$, pressure $P_\infty = 26000$ Pa, and temperature $T_\infty = 206$ K for all simulations. The corresponding Reynolds number per meter (R_e/D) was 15.2×10^6. Steady-state flow conditions were assumed. The computations were run at angles of attack (AOA) of 0, 10, 15, 17, 19, and 20 deg, and a zero roll rate was assumed for all cases.

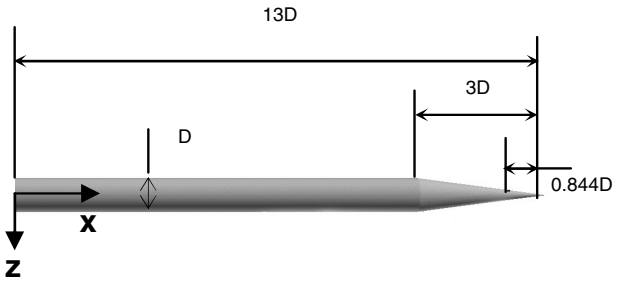

Fig. 1 Dimensions of the studied slender body.

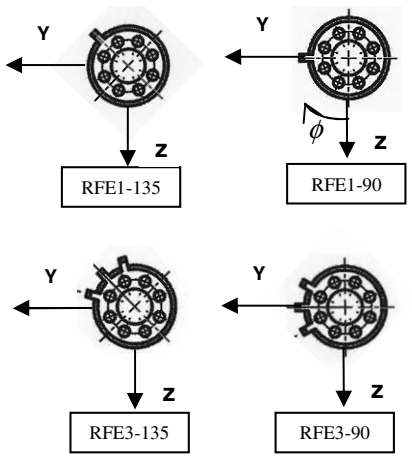

Fig. 2 Studied FE configurations viewed from the front of the missile.

III. Numerical Procedure and Grid Generation

The steady-flow numerical solutions were obtained using the research CFD code SPARC, developed at the University of Karlsruhe. It is a multiblock-structured code that uses the finite volume method to discretize the governing Navier–Stokes equations in space. An artificial dissipation term is included in the central-difference scheme to dampen computational instabilities. The explicit terms are evaluated using the Runge–Kutta method and the implicit terms are computed using the modified lower-and-upper decomposition method developed by Jameson and Turkel [4] and Jameson and Yoon [5]. A multigrid strategy is available to accelerate the computations, and the code has been parallelized. There are several turbulence models available, such as the Spallart–Allmaras and Baldwin–Lomax one-equation models, Lauder and Sharma's k-ε model, and Spezial's nonlinear k-τ model. Previous exercises in [6] indicated that the Spallart–Allmaras one-equation turbulence model in the code is quite robust. It was therefore used to perform the numerical simulations for the FE study presented in this paper.

The multiblock-structured meshes were produced using ICEM-CFD HEXA [7]. An H-grid topology was used to wrap the mesh around the slender body, as shown in Fig. 3, for the configuration with three FEs. Fine grids were used to resolve the boundary layer above the viscous walls. The average dimensionless normal distance of the first grid point from the wall, y^+, was less than two. The total number of grid points was about 3 million. In these calculations, the governing equations were solved through the viscous layer to the wall of the generic body. The base flow was neglected.

All computations were run on the Challenger cluster at the Aerodynamics Laboratory at NRC–IAR. A parallel technique was used to speed up the computations. All variables converged and their residuals were reduced by approximately four orders of magnitude.

IV. Experimental Descriptions

The measurements were performed in the trisonic wind tunnel at DRDC Valcartier. This is an in-draft tunnel with a test-section cross-sectional area of 0.6 by 0.6 m. Typical run times vary between 5 and 11 s, depending at which Mach number the wind tunnel is operated. The turnaround time between the runs is about 30 min. The test-section Mach number can be varied from 0.2 to 4.0 by interchanging the test-section bidimensional nozzle blocks. For the current study, tests were performed at a freestream Mach number of 1.5. The corresponding Reynolds number per meter at this Mach number was about 15.2×10^6. The force measurements were performed using a six-degree-of-freedom, 0.75-in., Able MK-XIX-C balance.

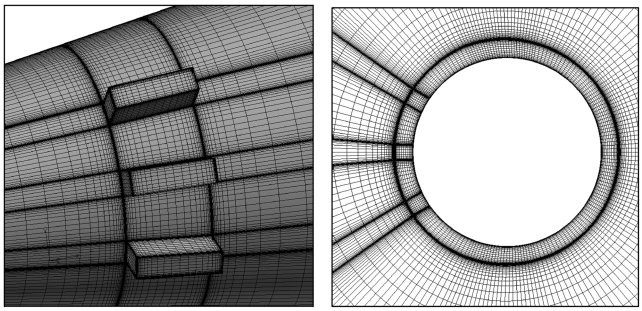

Fig. 3 Close-up views of the mesh for the RFE3-90 configuration.

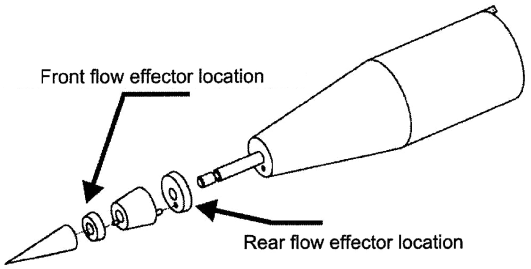

Fig. 4 Wind-tunnel model setup.

For the wind-tunnel model, the nose of the slender body was equipped with disks onto which the different flow-effector configurations were mounted, as shown in Fig. 4. These disks were located at the front and rear flow-effector rows. One disk was manufactured for each flow-effector configuration tested. Some of the different flow-effector configurations are shown in Fig. 2. The nose-disk assembly was designed such that the disks could be indexed in 45-deg steps.

The measurement uncertainty of the test-section Mach number was estimated to be $\pm 1.1\%$ of the calculated value. The uncertainty of the aerodynamic coefficients corresponding to a 95% confidence limit (run-to-run variations) were $\pm 1.7\%$ for the normal force coefficient, $\pm 1.3\%$ for the pitching moment coefficient, $\pm 3.0\%$ for the axial force coefficient, and $\pm 3.0\%$ for the side force coefficient [8]. For a detailed experimental description, refer to [9].

V. Results and Discussion

To evaluate the calculation errors introduced by the different grid distributions, computations were run for the following two sets of grids for the baseline body-alone configuration. One is a uniform grid distribution in the angular direction shown in Fig. 5; the other is the same grid distribution that was used for the missile with FEs, shown in Fig. 6.

The side force coefficients C_Y computed using the preceding two meshes are listed in Table 1. The ratio of the side to normal force coefficients are also listed in the table. For the body-alone configuration, theoretically speaking, the side force should be zero. The results shown in the table represent the numerical errors for the current computations. For the nonuniform mesh, the numerical error was about 0.025 for the side-force-coefficient predictions, which is about 1.3% of the normal force coefficients.

Figure 7 presents the computed streamlines for the flow past the nose of the missile body for the RFE1-135 configuration at AOA $= 17$ deg. Initially, the flow was attached to the nose section, but owing to the sizeable angle of attack, the flow was directed around the cylindrical conical surface and eventually separated from the surface. The separation developed two distinct systems of vortices that were typical in overall terms to the flow behavior noted in experimental and computational results reported in the literature [10]. The flow effector, which was located only on the starboard side of the nose cone, triggered the starting vortex, causing it to twist, stretch, and grow in size. Consequently, the vortices on the side containing the FE were larger than the vortices on the other side of the body. Figure 8 shows a close-up of the pressure field on the surface of the body around the FE. High-pressure regions were identified on the bottom and leading surfaces of the FE.

To assess the streamwise influence of the flow effectors, it is important to inspect the axial pressure distribution downstream of the devices. Figure 9 displays the surface-pressure distributions on top of

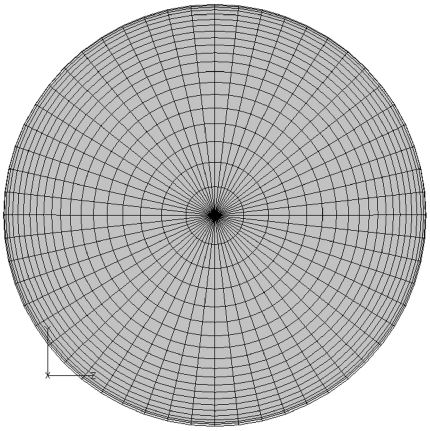

Fig. 5 Nose view of the uniform mesh for body-alone configuration.

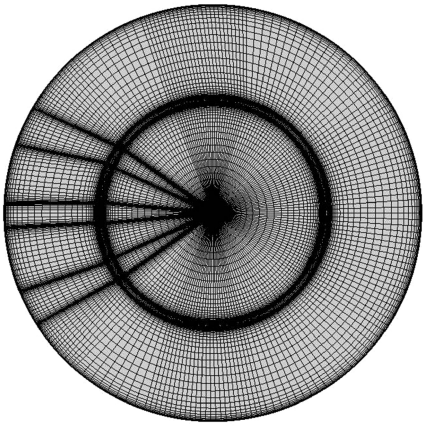

Fig. 6 Nose view of the nonuniform FE mesh for body-alone configuration.

the body alone and the single FE at $\phi = 135$-deg configurations. Apart from the noticeable drop in pressure behind the device, the pressure magnitude on the starboard side of the body-alone case is somewhat smaller than the corresponding pressure magnitude for the configuration with the FE. Figure 10 compares the surface-pressure field on the remaining region for the configurations with and without the flow effector. In addition to the obvious difference in pressure fields, the asymmetric pressure as a result of installing the flow effector contributed to the resultant side force.

Figure 11 presents the integrated side force coefficients for the RFE1-135 configuration. The reference area used to nondimensionalize the forces was the base area of the cylindrical body. The wind-tunnel data obtained by DRDC Valcartier are also included in these figures. The solid symbols show the results obtained from the computations and the hollow symbols indicate the corresponding experimental results. The numerical side force coefficients agreed well with the experimental data. Both the numerical and experimental data revealed that the maximum side force occurred near AOA $= 17$ deg. Similar observations were made for the side force moment coefficients, as shown in Fig. 12.

Comparisons between the numerical and experimental normal and axial force coefficients for various configurations are shown in Figs. 13 and 14, respectively. Because the base flow was not computed in the current CFD results, the axial force coefficients

Table 1 Side force coefficients computed using the uniform and nonuniform meshes for the body-alone configuration

	Uniform mesh		Nonuniform mesh	
AOA $= 15$ deg	$C_Y = -0.00358$	$C_Y/C_N = -0.00280$	$C_Y = -0.02033$	$C_Y/C_N = -0.01288$
AOA $= 17$ deg	$C_Y = -0.00567$	$C_Y/C_N = -0.00335$	$C_Y = -0.03043$	$C_Y/C_N = -0.01455$

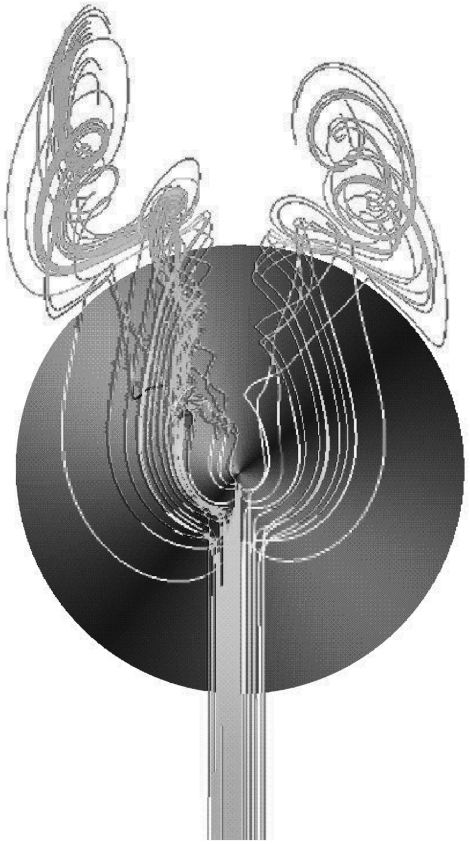

Fig. 7 Streamlines past the slender body for RFE1-135 at AOA = 17 deg.

shown in Fig. 14 were obtained from the CFD axial force on the body surface added to the axial base forces calculated using the empirical code Missile Datcom [11]. In general, the numerical normal force coefficients were about 10% greater than the wind-tunnel data for angles of attack greater than 15 deg. The numerical axial force results, however, were in a good agreement with the wind-tunnel data and did not change much when the AOA was increased.

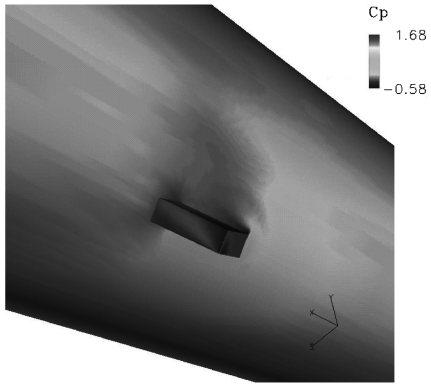

Fig. 8 Surface pressure on the slender body around the FE for RFE1-135 at AOA = 17 deg.

Figure 15 shows the predicted centers of pressure in the axial direction. The reference location of X_{cp} was the base of the missile body. The numerical data agreed well with the wind-tunnel data, and they both indicate that the center of pressure moved toward the missile base as the AOA was increased.

To analyze the efficiency of the FE devices, ratios of the numerical side to normal forces are plotted in Fig. 16. The flow effector of the RFE1-135 configuration provided side forces that were, on average, about 25% of the normal forces when the AOA was at 10 and 15 deg. The side force gain was quite remarkable for such a small device installed on the nose of the cone section. Note that even though the maximum side force occurred at AOA = 17 deg, the ratio of the side to normal forces started to drop after AOA = 15 deg.

To investigate how the various features of the flow effectors affected the missile's aerodynamic performance, the following parametric studies were performed.

A. Effect of the Azimuthal Location of the Flow Effectors

Computations were performed for a single FE at the front axial location with various azimuthal angles along the starboard side of the body when the AOA = 17 deg. The side-force-coefficient results are shown in Fig. 17. The FE situated at $\phi = 135$ deg provided the largest side force. The side force gradually decreased as the FE position moved to the horizontal symmetry plane of the body ($\phi = 90$ deg).

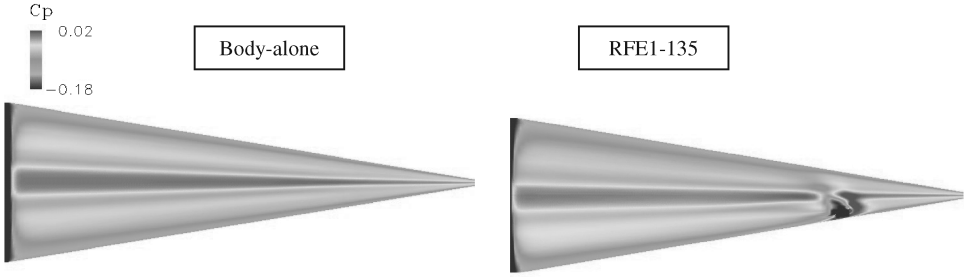

Fig. 9 Top view of the surface pressures on the cone sections of the body-alone and RFE1-135 configurations at AOA = 17 deg.

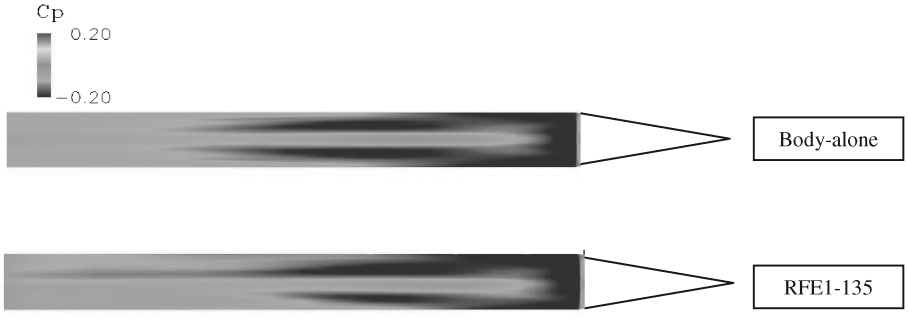

Fig. 10 Top view of the surface pressures on the cylinder sections of the body-alone and RFE1-135 configurations at AOA = 17 deg.

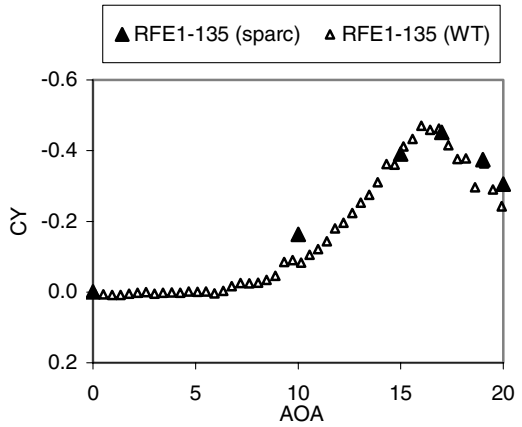

Fig. 11 Variation of the side force coefficients with angle of attack for RFE1-135.

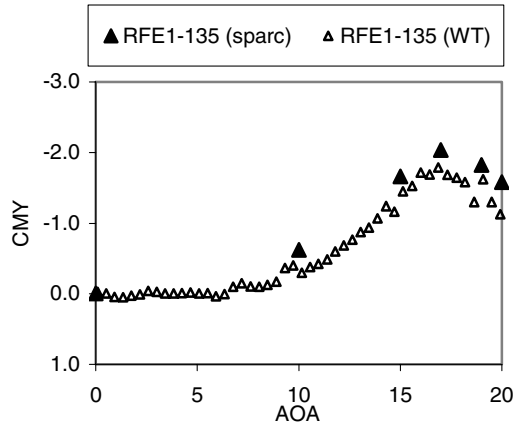

Fig. 12 Variation of the side-moment coefficients with angle of attack for RFE1-135.

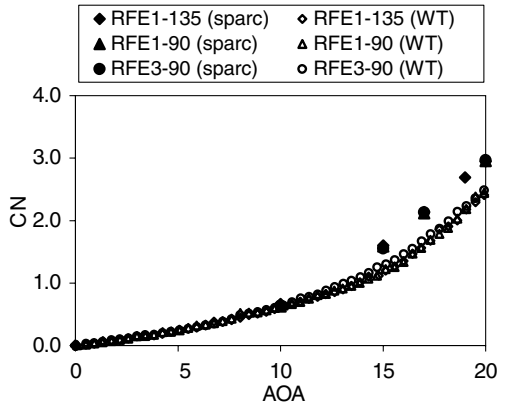

Fig. 13 Variation of the normal force coefficients with angle of attack.

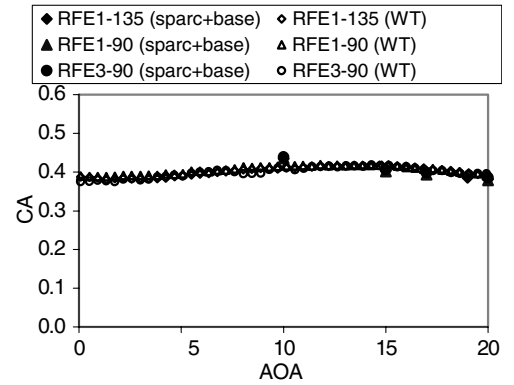

Fig. 14 Variation of the axial force coefficients with angle of attack.

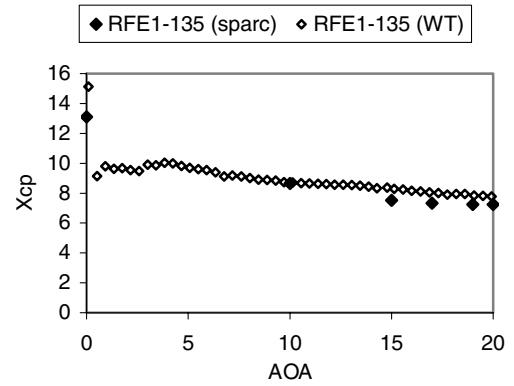

Fig. 15 Variation of the centers of pressure in the axial direction with angle of attack.

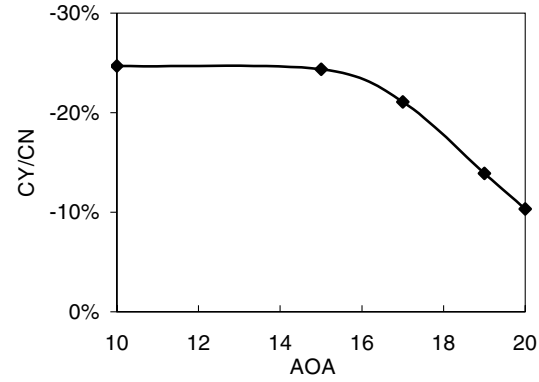

Fig. 16 Variation of the ratio of the side to normal forces with angle of attack for RFE1-135.

When the FE was located on the upwind side of the missile ($f = 60$ deg) or close to 160 deg, its contribution to side force was insignificant.

Figure 18 shows the velocity vectors at the cross-sectional plane corresponding to $x_n/D = 5.417$ for three configurations: RFE1-135, RFE1-90, and RFE0. We assumed that at the calculated AOAs, the separation flow is stable and the vortex pair location is time-independent. For the body-alone configuration RFE0, the two vortex systems above the missile were symmetric. For the configurations with flow effectors, the vortex system on the side with the flow effectors was obviously disturbed. The affected vortex system seemed to be "pushed" up, away from the body. Comparing the vortex systems of the configurations of RFE1-135 and RFE1-90, the disturbance caused by the flow effector with $\phi = 135$ deg is more important than that caused by the flow effector with $\phi = 90$ deg. In fact, it produced the largest side force among all the investigated configurations (Fig. 17).

Figure 19 shows the pressure coefficient predictions around a cross section located just downstream of the flow effectors for the RFE-135 and RFE1-90 configurations with AOA = 17 deg. The angle of phi in the figure was defined as the angular distance from the bottom of the slender body along either the port and or starboard sides of the missile. The thick curves indicate data on the starboard side on which the FEs were located, and thin curves indicate data on the port side, which did not have any FEs. Because the studied geometry was symmetric, the surface pressures on either side should be identical for the configuration without FEs, apart from very small numerical errors arising from the asymmetric grid distributions. Thus, the difference between the thick and thin curves determines the pressure side forces caused by the FEs.

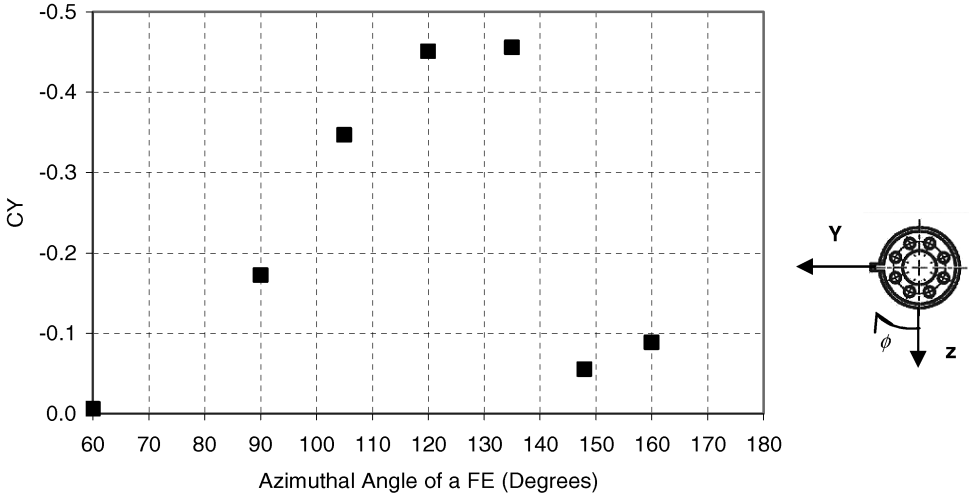

Fig. 17 Variation of the side force coefficient with azimuthal angle for a single FE at AOA = 17 deg.

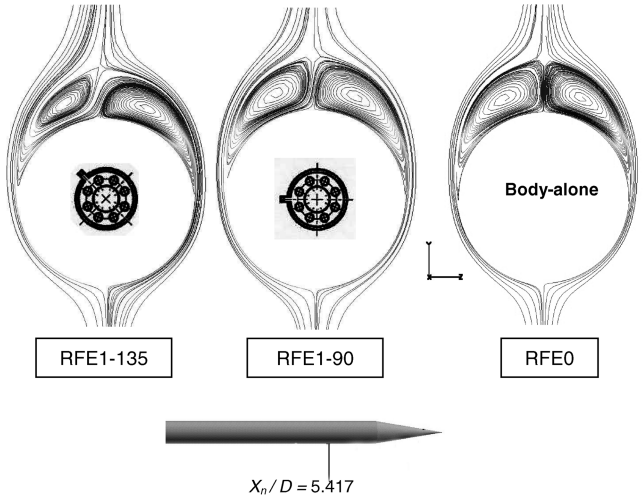

Fig. 18 Velocity vectors at a cross section located at $x_n/D = 5.417$ downstream from the tip of the missile at AOA = 17 deg.

The flow effector of the RFE1-135 configuration mostly changed the upper body surface pressure and had little effect on the surface pressures of the lower half of the missile. However, the pressure change caused by the flow effector of the RFE1-90 configuration on the lower half of the body was quite obvious. In the figure, the large dip in the pressure between 60 and 90 deg would also reduce the total side force on the missile body.

Figure 20 shows the pressure coefficients around a cross section located at $x_n/D = 6.625$ downstream of the flow effectors with AOA = 17 deg for both of the configurations. Both cases showed a consistent positive pressure difference between the sides with and without the FEs. But in general, at $x_n/D = 6.625$, the pressure difference for the RFE1-135 configuration was greater than that of the RFE1-90 configuration. Consequently, the maximum integrated side force coefficient of RFE1-135 was 55% greater than that of RFE1-90.

B. Effect of the Axial Location of the Flow Effectors

Two axial locations of the flow effector were studied: the front position located at $x_n/D = 0.844$ from the tip of the nose and the back position located at $x_n/D = 1.268$. Figure 21 shows the numerical and the wind-tunnel side force coefficients for these two positions with one flow effector at $\phi = 135$ deg. Again, the numerical data agreed well with the wind-tunnel data, except for RFE1-back-135 at AOA = 14 deg. The reason for the RFE1-back-135 discrepancy has not been determined and remains a subject for future investigation. The maximum side force produced by the front FE configuration was at AOA = 17 deg. For the back FE configuration, the maximum side force location was shifted to close to AOA = 14 deg, and its computed magnitude was only 25% of the front configuration (cf. 60% for the experiment). The vortex system for the body-alone configuration is shown in Fig. 7, stretched away from the missile body in the axial direction. In this way, the FE at the front position was closer to the vortex system than the FE at the back position. The front configuration, therefore, was more efficient than the back configuration in influencing the vortex system behavior.

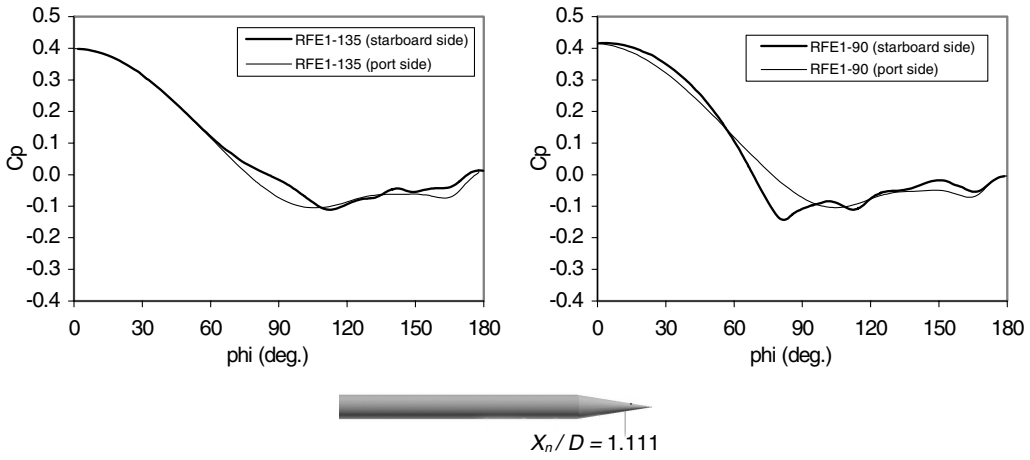

Fig. 19 Pressure coefficients at $x_n/D = 1.111$ with AOA = 17 deg. Thick curves correspond to the starboard side of the missile (with FEs), and thin curves correspond to the port side of the missile (without FEs).

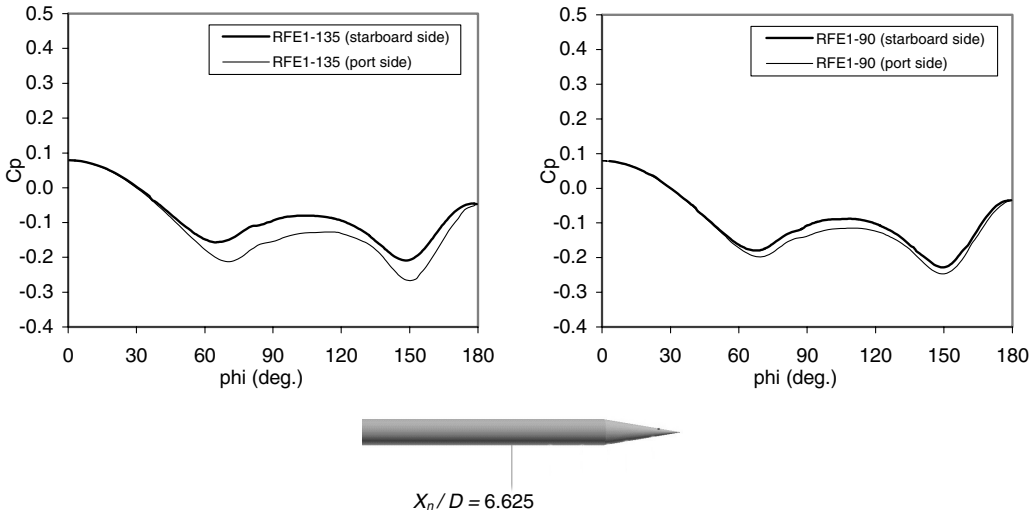

Fig. 20 Pressure coefficients at $x_n/D = 6.625$ with AOA = 17 deg. Thick curves correspond to the starboard side of the missile (with FEs), and thin curves correspond to the port side of the missile (without FEs).

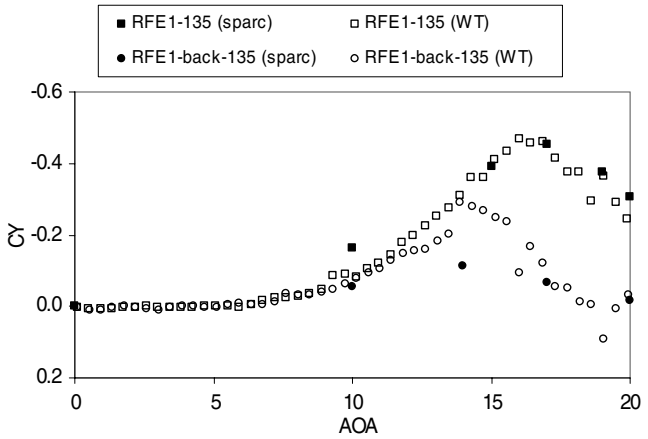

Fig. 21 Comparison of the side force coefficients between the configurations with a single FE at the front and back axial locations at AOA = 17 deg.

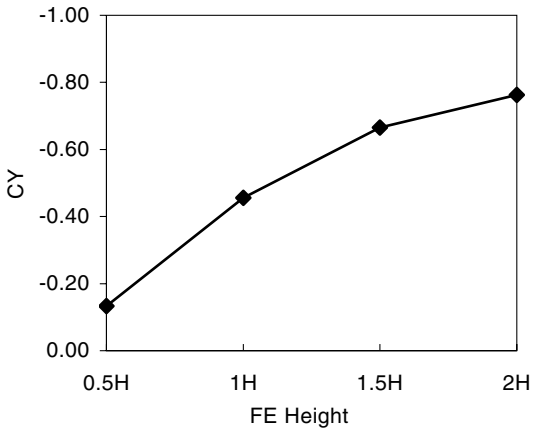

Fig. 22 side force coefficients vs height of the flow effector.

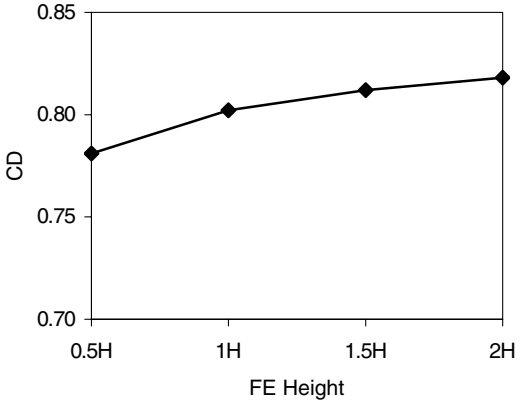

Fig. 23 Drag coefficients vs height of the flow effector.

C. Effect of the Height of the Flow Effectors

Numerical investigations were performed for a single-FE configuration at the front position with an azimuthal angle of 135 deg, with several different flow-effector heights: 0, 0.5, 1, 1.5, and $2H$, where $H = 0.033D$. The numerical side force coefficients for these configurations, shown in Fig. 22, indicate that the induced side force increased with the flow-effector height. The largest rate of increase occurred at a flow-effector height of $1H$. The ratio of the side over the normal force (C_Y/C_N) for the four flow-effector heights 0.5, 1, 1.5, and 2 was −6.43, −21.34, −30.77, and −35.02%, respectively.

The ratio jumped 15% when the height changed from 0.5 to $1H$. However, the increased height of the flow effector also brought about negative effects in the drag coefficients (Fig. 23); for instance, the drag coefficient increased about 3% from 0.5 to $1H$. Considering the mechanism required to move the flow effector, which should extract in and out of the missile body, a smaller flow effector is more desirable in terms of the missile weight and volume design. A best-compromised height might be $1H$.

D. Effect of the Number of Flow Effectors

Triple-FE configurations were also studied to investigate the effect of the number of the flow effectors. The middle FE was located at the positions corresponding to the single-FE configuration, 135 and 90 deg, and the other two FEs were positioned 30 deg on either side of the central FE.

Figure 24 compares the side force coefficients of the configurations with the flow effectors situated at an azimuthal angle of 90 deg. Both the numerical and experimental results revealed that the triple-FE configuration RFE3-90 improved the side force significantly over the corresponding single-FE configuration RFE1-90. Because the side force of a single flow effector at $f = 120$ deg was 61.7% greater than at $\phi = 90$ deg (see Fig. 17), the top FE of the RFE3-90 triple configuration, which was also located at 120 deg, was expected to contribute greatly to the increase of the side force coefficient.

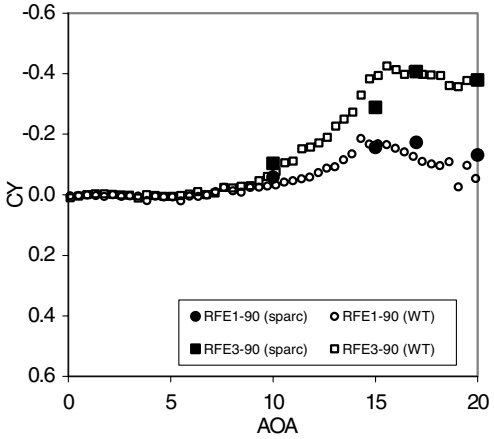

Fig. 24 Variation of the side force coefficients with angle of attack for the single-FE and triple-FE configurations at $\phi = 90$ deg.

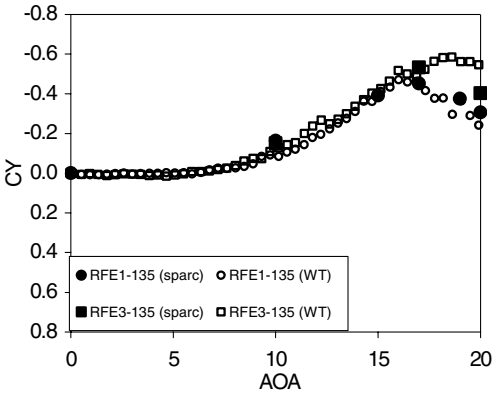

Fig. 25 Variation of the side force coefficients with angle of attack for the single-FE and triple-FE configurations at $\phi = 135$ deg.

For the RFE3-135 triple-FE configuration, the top FE was located at $\phi = 165$ deg, a position that did not produce a noticeable side force in Fig. 17, but the bottom FE, which was located at $\phi = 105$ deg, was expected to contribute to the increased side force to a certain level. Consequently, even though the RFE3-135 configuration improved the side force coefficient over the RFE1-135 configuration, the improvement was not as significant as that found for the RFE3-90 over the RFE1-90 configurations (Fig. 25).

The side force did increase with the number of FEs. However, the advantage was not dramatic, especially considering the complexity of the mechanism design requirement for multiple FEs.

VI. Conclusions

Numerical studies were performed for the flow past a generic missile body at $M = 1.5$ with flow effectors installed on the conical forebody. The main purpose of this exercise was to investigate whether miniature flow effectors could be placed on the forebody to generate sufficient side forces for lateral control. Parametric studies were performed considering the effects of the locations, numbers, and dimensions of the flow effectors on the magnitude of the side force. The numerical and wind-tunnel results indicated that the maximum peak side forces occurred at AOA = 17 deg for all the configurations with flow effectors at the front axial location $x_n/D = 0.844$. Among the configurations studied, the single FE situated at an azimuthal angle of 135 deg was the most efficient at generating the side forces. These quantitative observations agreed with the wind-tunnel results obtained from DRDC Valcartier. Regarding the quality of the comparison, the numerical force coefficients agreed well with the wind-tunnel data.

Both numerical and experimental studies concluded that for the studied cases, the location of FEs was more important than the number of FEs in terms of their contribution to the side force. The numerical study also showed that the side forces generated by the RFE1-135 configuration were, on average, about 25% of the normal forces. The side force gain was quite remarkable with such a small device installed at the nose of the body. This supports the idea of using small devices at the nose of the slender body to control the side forces.

Acknowledgments

The current work was partly sponsored by the Technology Investment Fund through Defence Research and Development Canada—Valcartier. The authors would like to acknowledge the advice provided by Francois Lesage, Frank Wong, and Mahmood Khalid. The authors would also like to acknowledge F. Magagnato of the Department of Fluid Machinery of the University of Karlsruhe, who developed the computational fluid dynamics research code SPARC.

References

[1] Patel, M. P., Prince, T. S., Carver, R., DiCocco, J. M., Lisy, F. J., and Ng, T. T., "Deployable Flow Effectors for Phantom Yaw Control of Missiles at High Alpha," AIAA Paper 2002-2827, 2002.

[2] Patel, M. P., Prince, T. S., Ng, T. T., DiCocco, J. M., and Lisy, F. J., "MEMS Actuated Deployable Flow Effectors System for Missile Control," Orbital Research, Inc., Rept. AD-a386 547, Cleveland, OH, 2000.

[3] Garon, K. D., Abate, G. L., and Hathaway, W., "Free-Flight Testing of Generic Missile with MEMS Protuberances," AIAA Paper 2003-1242, 2003.

[4] Jameson, A., and Turkel, E., "Implicit Schemes and LU-Decomposition," *Mathematical Computations*, Vol. 37, No. 156, 1981, pp. 385–397.

[5] Jameson, A., and Yoon, S., "LU-Implicit Schemes with Multiple Grids for the Euler Equations," AIAA Paper 86-0105, 1986.

[6] McIlwain, S., and Khalid, M., "Fluid Dynamic Analysis of Non-Traditional Supersonic Projectiles," *Canadian Aeronautics and Space Journal*, Vol. 52, No. 2, 2006, pp. 47–57.

[7] ANSYS ICEM CFD, Software Package, Ver. 4.3.1, ICEM CFD Engineering, Berkeley, CA, Oct. 2003.

[8] Girard, B., "Wind Tunnel Tests on DREV-ISL Reference Models at Supersonic Speeds (Series ISLFPWT-1)," Defence Research Establishment Valcartier, Rept. DREV TM-9704, Quebec, Canada, 1997.

[9] Corriveau, D., "Impact of Nose-Mounted Micro-Structures on the Aerodynamics of a Generic Missile," Defence Research and Development Canada—Valcartier, TM 2004-310, Quebec, Canada, 2004.

[10] "Missile Aerodynamics," Research and Technology Organization, Rept. RTO-MP-5, Neuilly-sur-Seine, France, 1998.

[11] Blake, W. B., "Missile Datcom: User's Manual," U.S. Air Force Research Lab., Air Vehicles Directorate, Rept. AFRL-VA-WP-TR-1998-3009, Wright–Patterson AFB, OH, 1998.